Supporting Information:

Non-idealities in lab-scale kinetic testing: a theoretical study of a modular Temkin reactor

Gregor D. Wehinger,[*,†] Bjarne Kreitz,[‡] and C. Franklin Goldsmith[‡]

†*Institute of Chemical and Electrochemical Process Engineering, Clausthal University of Technology, Leibnizstr. 17, 38678 Clausthal-Zellerfeld, Germany*

‡*School of Engineering, Brown University, 184 Hope Street, Providence, Rhode Island 02906, United States*

E-mail: wehinger@icvt.tu-clausthal.de

Flow and species fields from CFD simulations

Fig. S1 and Fig. S2 show streamlines and velocity vector scenes for $\dot{V} = 50$ ml$_N$ min^{-1} in the top row and $\dot{V} = 200$ ml$_N$ min^{-1} in the bottom row for the sphere and ring catalyst pellet, respectively.
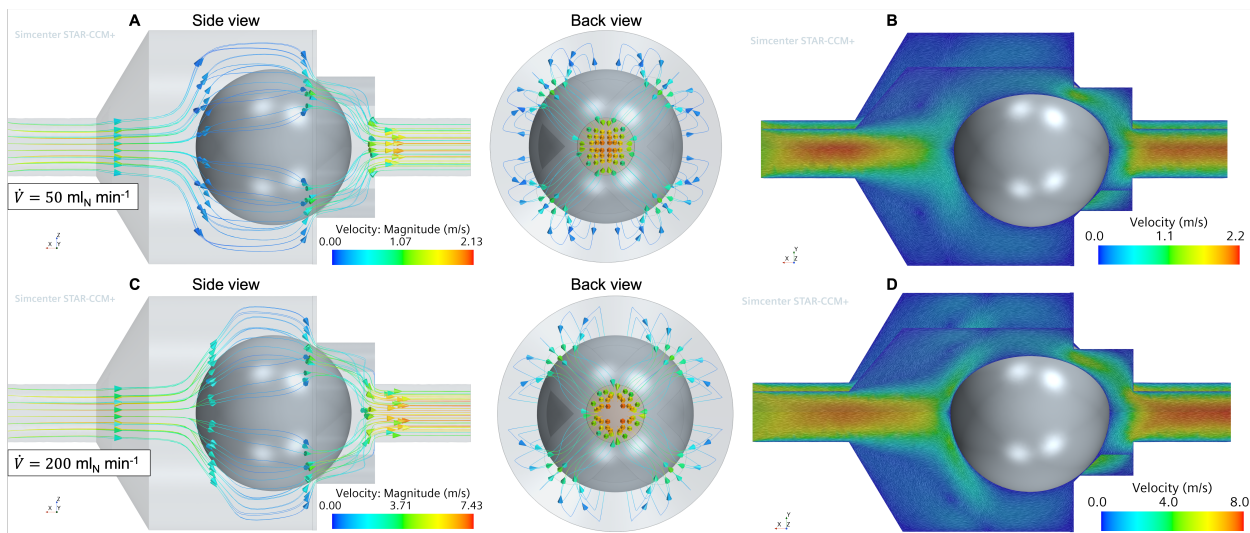

Figure S1: (A,C) Streamlines and (B,D) velocity vector scene for different volume flow rates: sphere catalyst pellet.
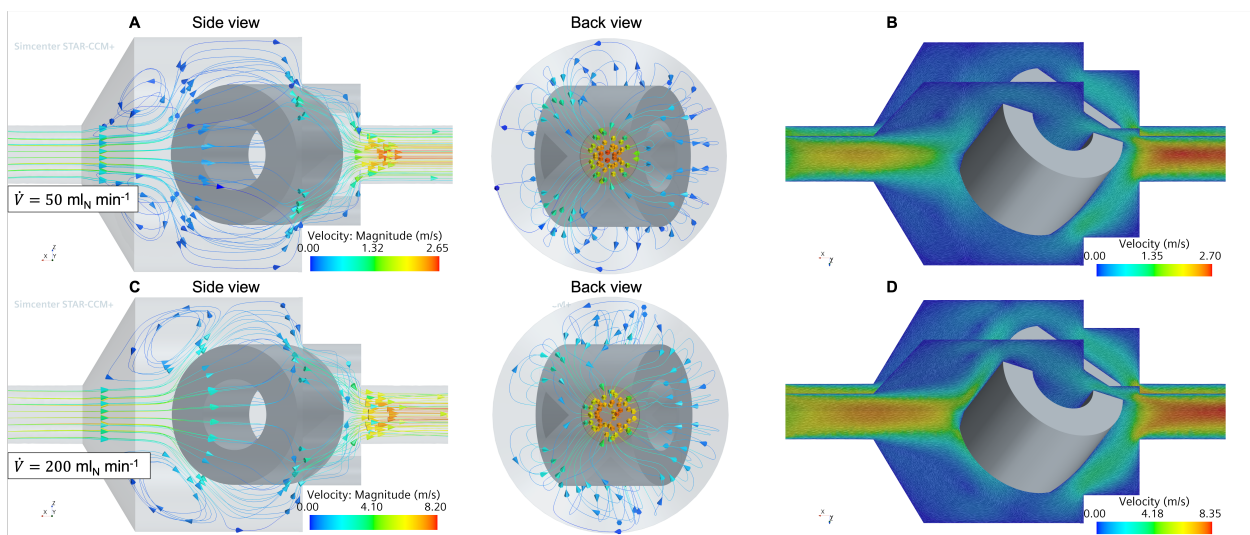

Figure S2: (A,C) Streamlines and (B,D) velocity vector scene for different volume flow rates: ring catalyst pellet.

Gas phase mole fractions are shown in Fig. S3 for $\dot{V} = 50$ ml$_N$ min^{-1} and for $\dot{V} = 200$ ml$_N$ min^{-1} in Fig. S4.
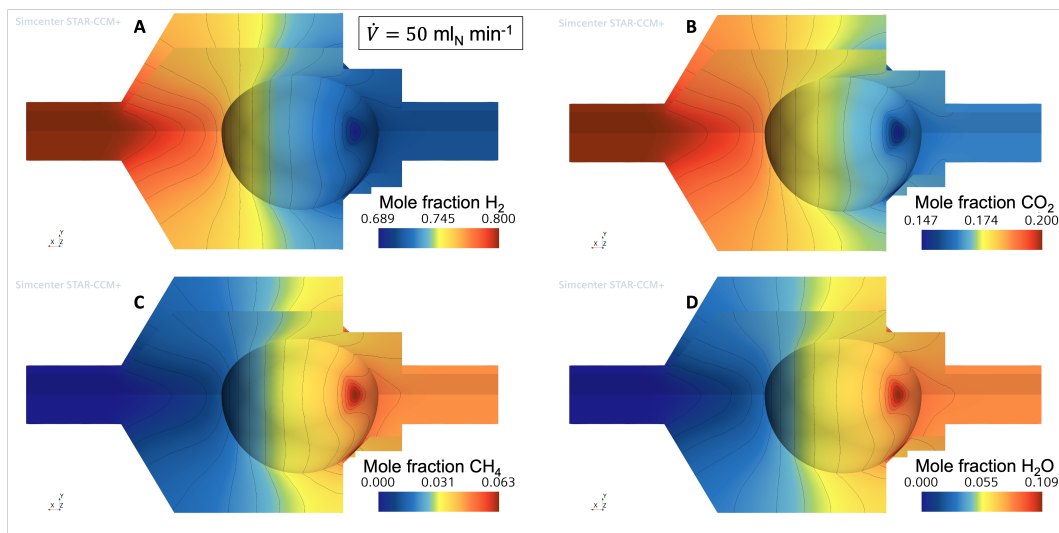

Figure S3: Sphere inside Temkin single chamber. Gas phase mole fractions at $\dot{V} = 50$ ml$_N$ min^{-1}: (A) hydrogen, (B) CO$_2$, (C) methane, (D) water.
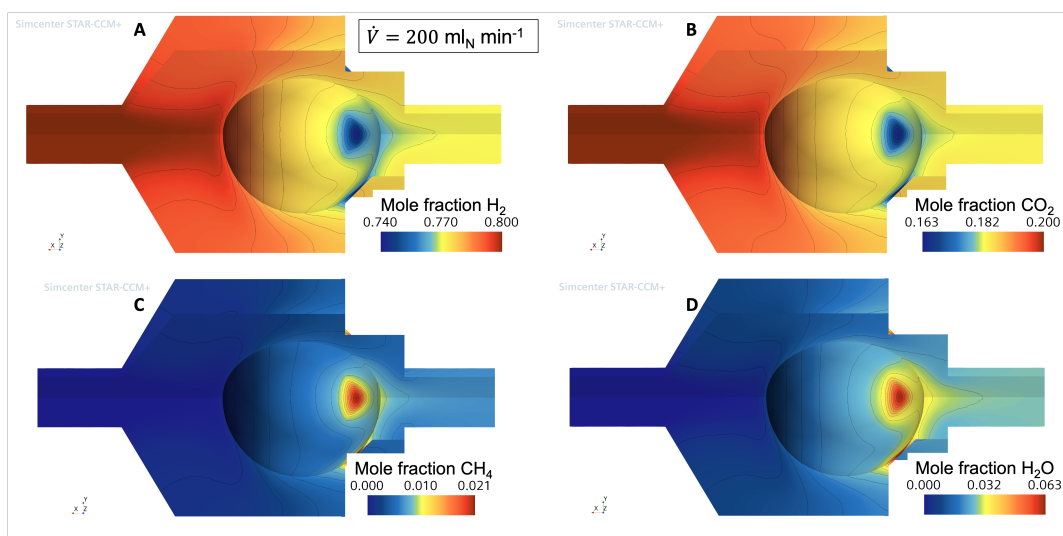

Figure S4: Sphere inside Temkin single chamber. Gas phase mole fractions at $\dot{V} = 200$ ml$_N$ min^{-1}: (A) hydrogen, (B) CO$_2$, (C) methane, (D) water.

Fig. S5 and Fig. S6 show adsorbed species surface fractions on the sphere for both volume flow rates.
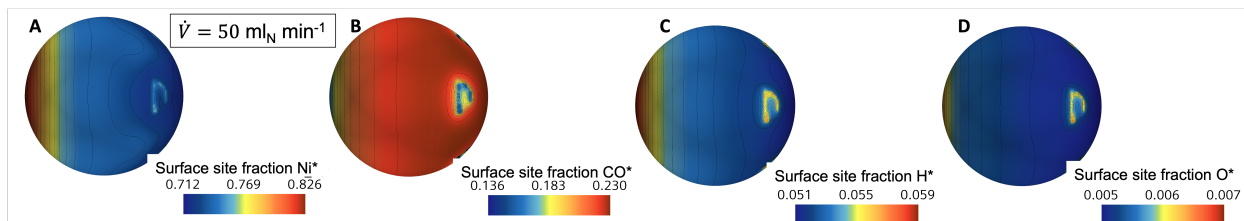

Figure S5: (A) Streamlines and (B) velocity vector scene at $\dot{V} = 50$ ml$_N$ min^{-1}.

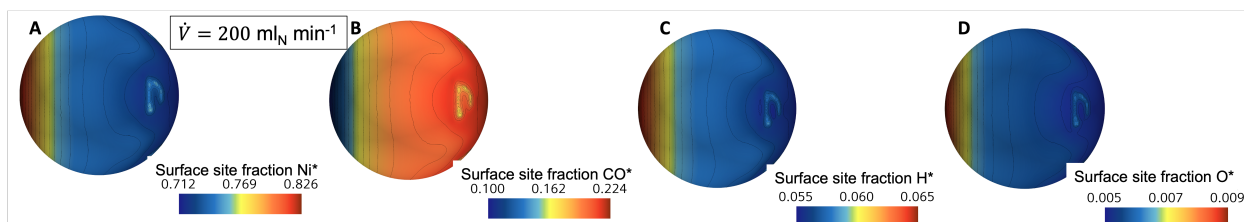
Figure S6: (A) Streamlines and (B) velocity vector scene at $\dot{V} = 50$ ml$_N$ min^{-1}.

The situation of gas-phase species distribution for the ring scenario is shown in Fig. S7 and Fig. S8.

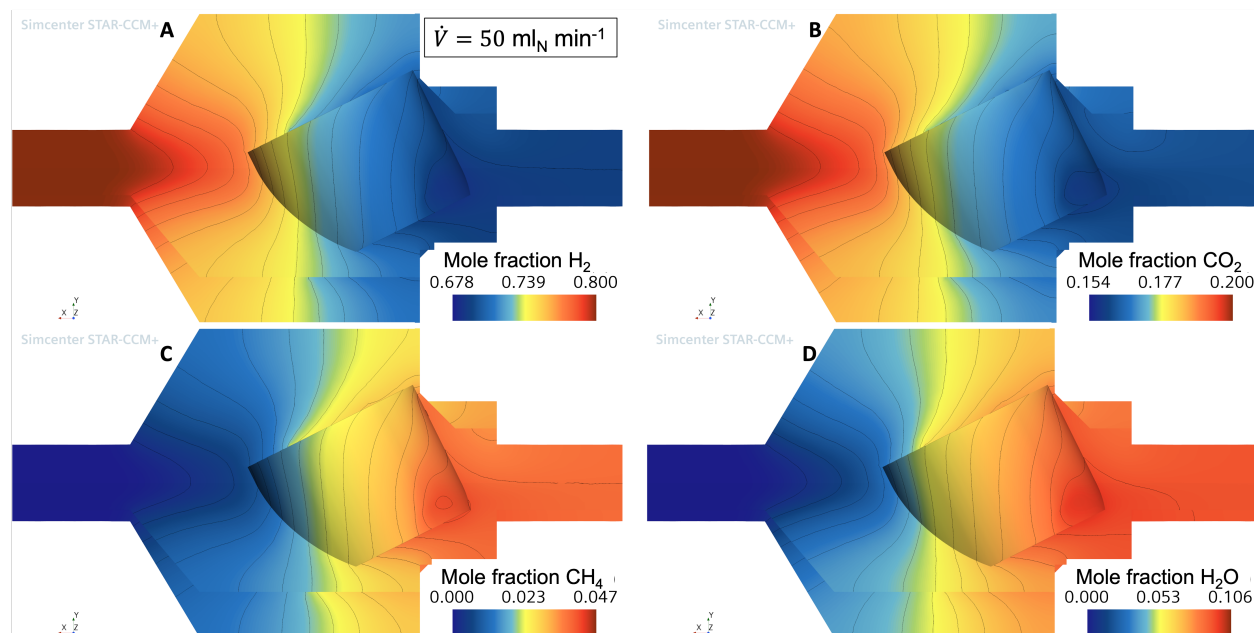Figure S7: Ring inside Temkin single chamber. Gas phase mole fractions at $\dot{V} = 50$ ml$_N$ min^{-1}: (A) hydrogen, (B) CO_2, (C) methane, (D) water.
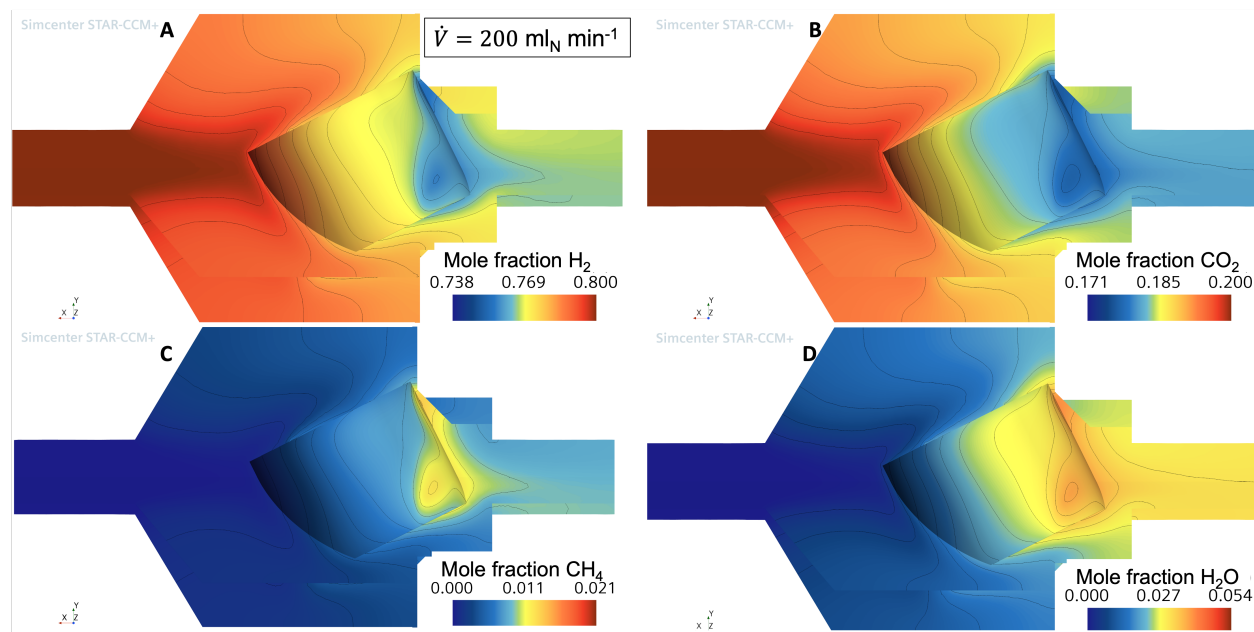

Figure S8: Ring inside Temkin single chamber. Gas phase mole fractions at $\dot{V} = 200$ ml$_N$ min^{-1}: (A) hydrogen, (B) CO_2, (C) methane, (D) water.

The adsorbed species for the ring is shown in Fig. S9 and Fig. S10.
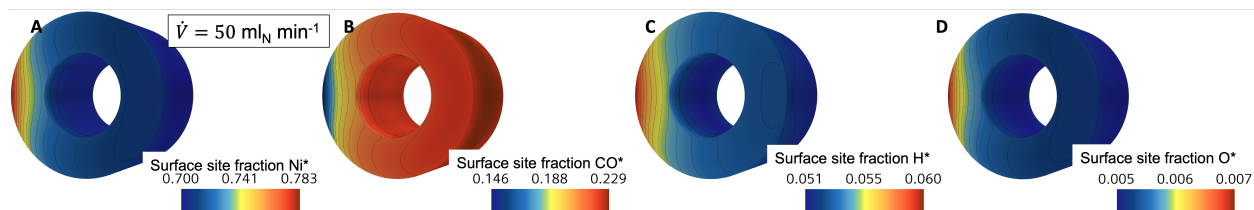

Figure S9: Ring inside Temkin single chamber. $\dot{V} = 50$ ml$_N$ min^{-1}.

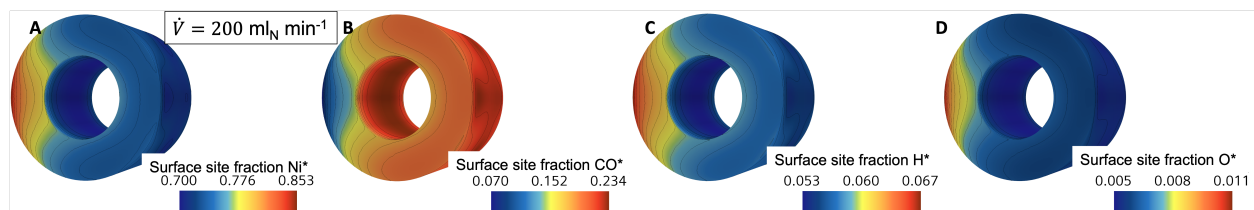Figure S10: Ring inside Temkin single chamber. $\dot{V} = 50$ ml$_N$ min^{-1}.

External mass transport evaluation

In Fig. S11 and Fig. S12, local Damköhler numbers are shown along the particle surface for different volumetric flow rates in the axial direction for the sphere and ring, respectively.
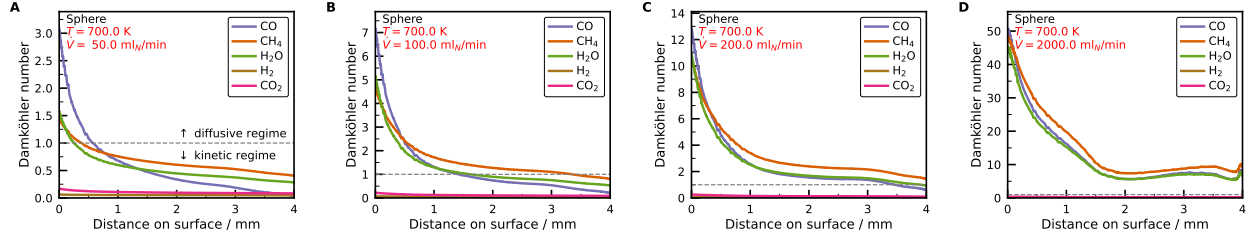

Figure S11: Damköhler number for sphere in Temkin single chamber. (A) $\dot{V} = 50$ ml$_N$ min^{-1}, (B) $\dot{V} = 100$ ml$_N$ min^{-1}, (C) $\dot{V} = 200$ ml$_N$ min^{-1}, and (D) $\dot{V} = 2000$ ml$_N$ min^{-1}.
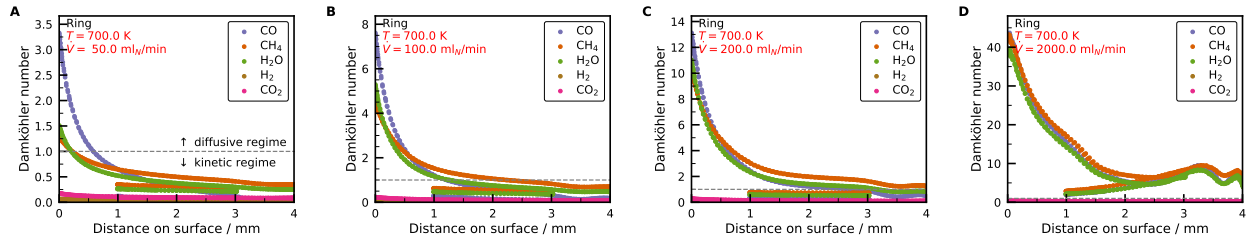

Figure S12: Damköhler number for sphere in Temkin single chamber. (A) $\dot{V} = 50$ ml$_N$ min^{-1}, (B) $\dot{V} = 100$ ml$_N$ min^{-1}, (C) $\dot{V} = 200$ ml$_N$ min^{-1}, and (D) $\dot{V} = 2000$ ml$_N$ min^{-1}.

Comparison between CFD and simplified models

The CFD results are compared with the ideal reactor models (CSTR and PFR) in Fig. S13 and Fig. S14.
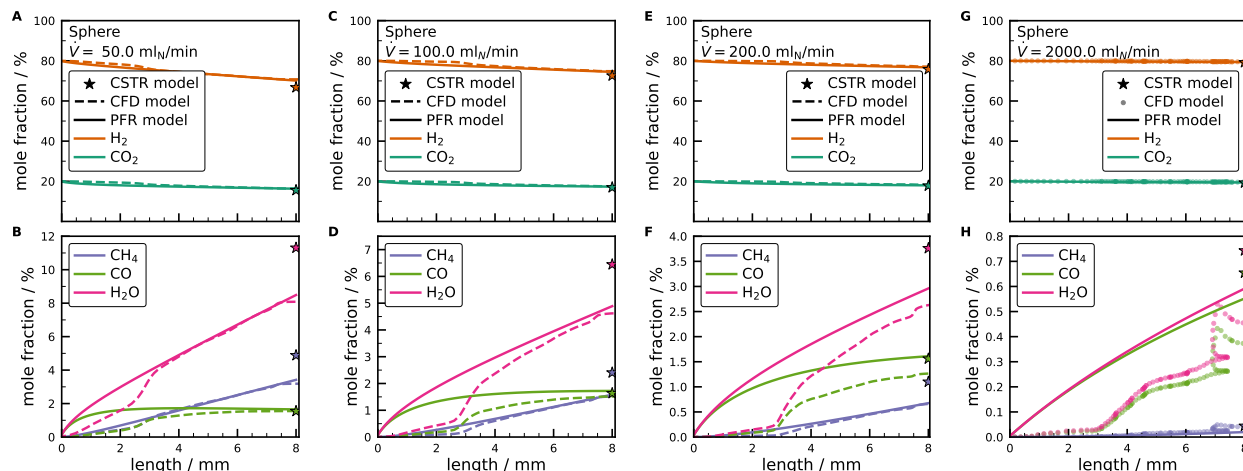

Figure S13: Sphere inside Temkin single chamber. Comparison between 1D PFR model, tanks-in-series (CSTR) model, and 3D CFD simulations of axial profiles of (top) reactants and (bottom) products mole fractions. (A,B) $\dot{V} = 50$ ml$_N$ min^{-1}, (C,D) $\dot{V} = 100$ ml$_N$ min^{-1}, (E,F) $\dot{V} = 200$ ml$_N$ min^{-1}, and (G,H) $\dot{V} = 2000$ ml$_N$ min^{-1}.
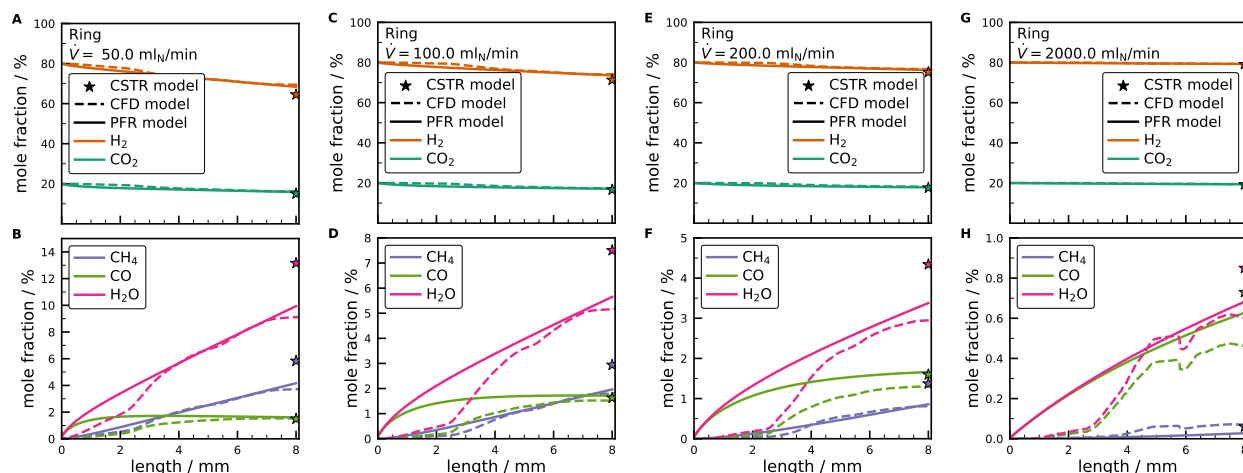

Figure S14: Ring inside Temkin single chamber. Comparison between 1D PFR model, tanks-in-series (CSTR) model, and 3D CFD simulations of axial profiles of (top) reactants and (bottom) products mole fractions. (A,B) $\dot{V} = 50$ ml$_N$ min^{-1}, (C,D) $\dot{V} = 100$ ml$_N$ min^{-1}, (E,F) $\dot{V} = 200$ ml$_N$ min^{-1}, and (G,H) $\dot{V} = 2000$ ml$_N$ min^{-1}.

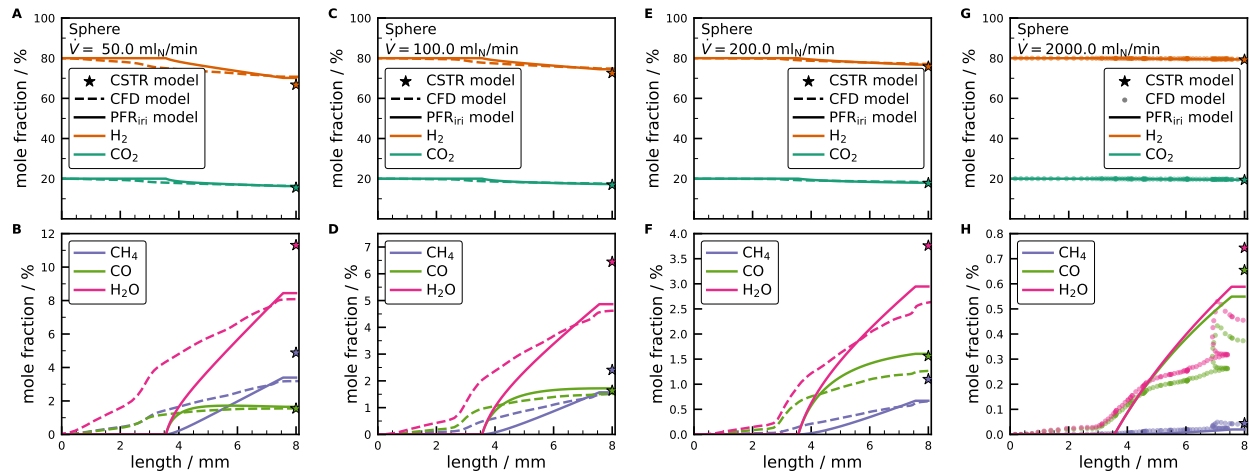Inert-active-inert PFR model results are shown in Fig. S15 and Fig. S16.

Figure S15: Sphere inside Temkin single chamber. Comparison between 1D PFR model inert-active-inert (PRF$_{iri}$), tanks-in-series (CSTR) model, and 3D CFD simulations of axial profiles of (top) reactants and (bottom) products mole fractions. (A,B) $\dot{V} = 50$ ml$_N$ min^{-1}, (C,D) $\dot{V} = 100$ ml$_N$ min^{-1}, (E,F) $\dot{V} = 200$ ml$_N$ min^{-1}, and (G,H) $\dot{V} = 2000$ ml$_N$ min^{-1}.
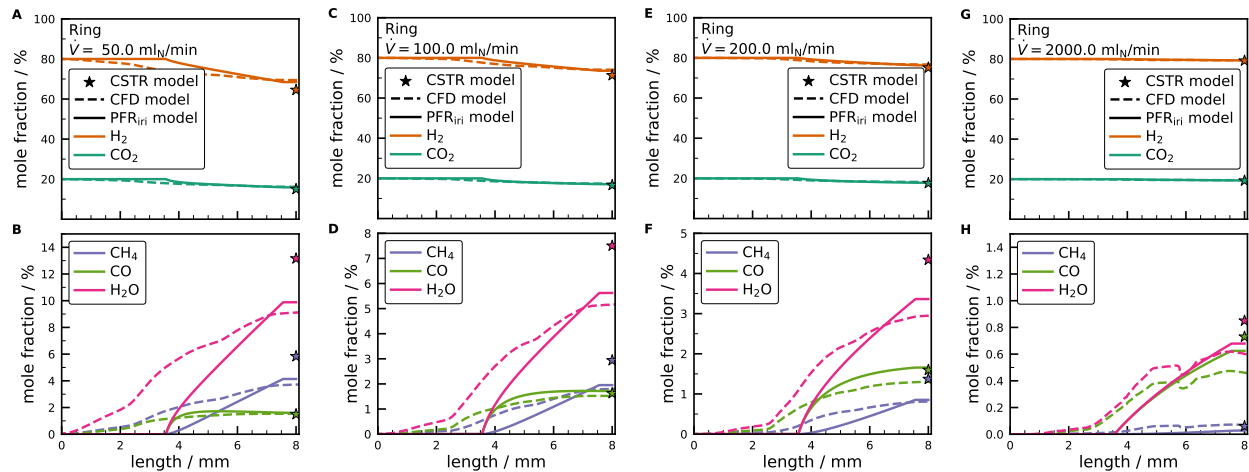

Figure S16: Ring inside Temkin single chamber. Comparison between 1D PFR model inert-active-inert (PRF$_{iri}$), tanks-in-series (CSTR) model, and 3D CFD simulations of axial profiles of (top) reactants and (bottom) products mole fractions. (A,B) $\dot{V} = 50$ ml$_N$ min^{-1}, (C,D) $\dot{V} = 100$ ml$_N$ min^{-1}, (E,F) $\dot{V} = 200$ ml$_N$ min^{-1}, and (G,H) $\dot{V} = 2000$ ml$_N$ min^{-1}.

Finally, the CFD results are compared with the CRN model, see Fig. S17 and Fig. S18.
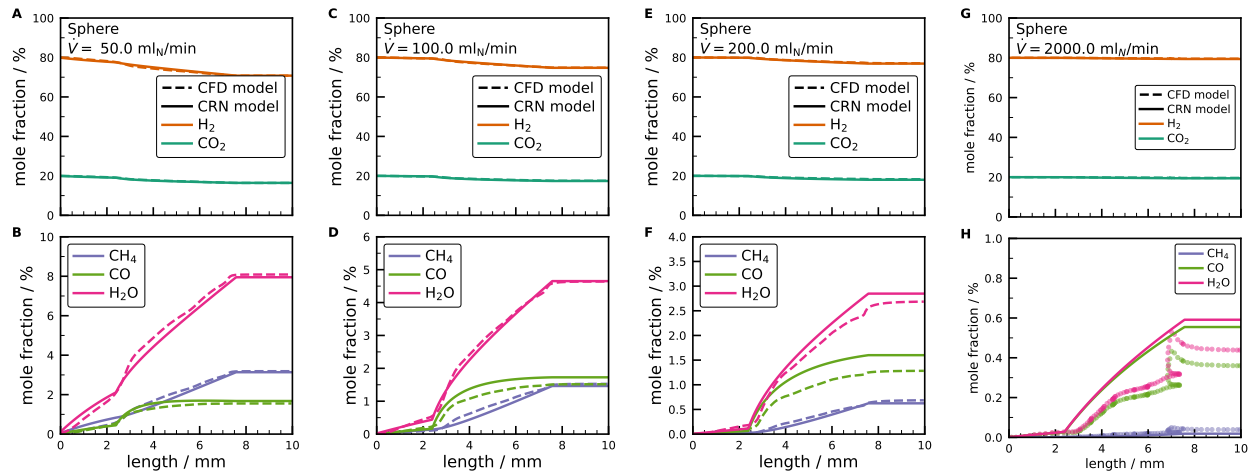

Figure S17: Sphere inside Temkin single chamber. Comparison between 1D CRN model and 3D CFD simulations of axial profiles of (top) reactants and (bottom) products mole fractions. (A,B) $\dot{V}$ = 50 ml$_N$ min^{-1}, (C,D) $\dot{V}$ = 100 ml$_N$ min^{-1}, (E,F) $\dot{V}$ = 200 ml$_N$ min^{-1}, and (G,H) $\dot{V}$ = 2000 ml$_N$ min^{-1}.
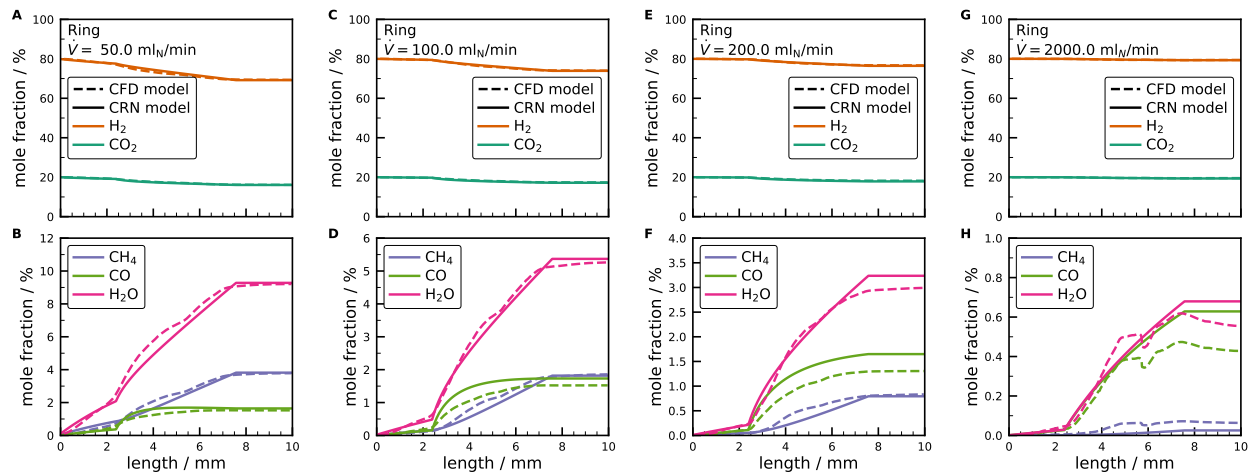

Figure S18: Ring inside Temkin single chamber. Comparison between 1D CRN model and 3D CFD simulations of axial profiles of (top) reactants and (bottom) products mole fractions. (A,B) $\dot{V}$ = 50 ml$_N$ min^{-1}, (C,D) $\dot{V}$ = 100 ml$_N$ min^{-1}, (E,F) $\dot{V}$ = 200 ml$_N$ min^{-1}, and (G,H) $\dot{V}$ = 2000 ml$_N$ min^{-1}.